VII International Conference on Particle-Based Methods
PARTICLES 2021
P. Wriggers, M. Bischoff, E. Oñate, M. Bischoff, A. Düster & T. Zohdi (Eds)

MODELLING AND EXPERIMENTAL ANALYSIS OF THE COOLING LIQUID FLOW IN EJECTOR DEEP DRILLING PROCESSES

DANILO CANINI[1], JULIAN F. GERKEN[2], DIRK BIERMANN[2] AND PETER EBERHARD[1]

[1]Institute of Engineering and Computational Mechanics (ITM)
University of Stuttgart
Pfaffenwaldring 9, 70569 Stuttgart, Germany
e-mail: danilo.canini@itm.uni-stuttgart.de

[2]Institute of Machining Technology (ISF)
TU Dortmund University
Baroper Str. 303, 44227 Dortmund, Germany

Key words: Ejector Deep Hole Drilling, Ejector Effect, Smoothed Particles Hydrodynamics, SPH, Deep Hole Drilling

Abstract. The efficient execution of demanding deep hole drilling operations represents, for manufacturing companies, a major challenge. The ejector method combines the advantages of deep hole drilling operations, such as high material removal rate and bore quality, with the convenience of the usage of conventional machining centers, since no specialized deep hole drilling machines with complex sealing systems are necessary. The ejector effect is responsible for a stable execution of the cutting process, providing the working zones with cooling lubricant. Achieving an enhanced understanding of flow effects and of process-specific peculiarities is fundamental for the appropriate design of the system. An experimental setup for in-process fluid pressure and volume flow measurement is developed, and, using the experimental measures as input data, a simulation model is developed applying the mesh-free Smoothed Particle Hydrodynamics method.

1 INTRODUCTION

Deep hole drilling methods allow the executions of bores with a large bore depth compared to the diameter, namely in drilling applications with a length-to-diameter ratio larger than $l/D > 10$. Different tools are available for the execution of deep bores.

The ejector method maintains the advantages of deep hole drilling, such as high material removal rate and high bore quality, on conventional machining centers. Different tool designs are used for drilling deep holes: tools with two symmetrically arranged cutting edges and tools with asymmetrical single-edge design, such as single-lip deep hole drill heads, ejector drilling with a double-tube system and BTA deep hole drilling with

a single-tube system. The asymmetrical design leads to self-centering of the tool in the bore by the use of guide pads [1]. In this paper the ejector deep hole drilling is considered. The ejector method maintains the advantages of deep hole drilling, such as high material removal rate and high bore quality, on conventional machining centers, since, unlike other deep hole drilling methods, no complex cooling lubricant sealing is necessary, therefore no special machines are required [2]. Due to the lack of process knowledge on the ejector effect, the cooling lubricant flow rate is often set to be higher than necessary during the operation, increasing the expenditure of resources and the process cost.

It is object of this research to achieve a better understanding of the behavior of an ejector deep hole drilling system, combining in-process sensor technology and simulations. The simulation scheme of choice is based on the Lagrangian method Smoothed Particle Hydrodynamics (SPH). The novel contribution of this paper lies in the fact that the study case presents a fluid flow with changing topology, combining free flows, fluid structure interaction with complex geometries and unusual pressure fields, thus making the more common simulation methods (finite element and finite volume methods) not applicable. The simulations, using as input the data coming from the experimental setup, will provide better understanding of the process while proposing optimization strategies that will then be verified and validated on an experimental rig.

2 PROCESS AND TOOL DESCRIPTION

A characteristic feature of deep hole drilling tools is their asymmetry in structure and the cutting edge arrangement, which creates the need for additional guide elements so that these can be used to support the resulting radial force components on the bore wall. The process-typical advantages of deep hole drilling, such as the very good surface quality and bore quality, are largely due to the use of the guide pads: on the one hand, these cause a levelling of the roughness peaks by plastic deformation and thus a smoothing of the bore [3], and on the other hand they limit the center run [4]. The design of the tool system is characterized by two concentric drill tubes, onto which the drill head is bolted. Figure 1 shows the schematic structure of an ejector deep hole drilling system. The supply of the cooling lubricant is indicated by the green arrows and the discharge by the red arrows.

The cooling lubricant is fed via a high pressure pump, a rotating tool connects the pump with the main spindle (Fig. 1C). The total supplied coolant flow $\dot{V}_{total}$ is divided (Eq. 1) into $\dot{V}_{AG}$, which will actually participate to the lubrication of the cutting area, and $\dot{V}_{EN}$, which will ensure the ejctor effect

$$\dot{V}_{total} = \dot{V}_{AG} + \dot{V}_{EN}, \tag{1}$$

$$\dot{V}_{AG} = \dot{V}_{IB} + \dot{V}_{loss}. \tag{2}$$

The coolant lubricant with volume flow $\dot{V}_{AG}$ is fed through the annular gap between the outer and inner tubes (Fig. 1B), exits near the machining zone through radial openings on the drill head and, in the case of a stable process with ejector effect the condition in Eq. (2) is fulfilled, the loss flow $\dot{V}_{loss}$ is small and the volume flow in the annular gap $\dot{V}_{AG}$ is nearly equal to the recirculated volume flow $\dot{V}_{IB}$ in the inner bar, and it is discharged

through the inner tube with the chips after flowing around the cutting edge area (Fig. 1A). If the ejector effect is not stable, a leakage occurs, and the cooling lubricant sprays into the machine. A part of the coolant lubricant with volume flow $\dot{V}_{EN}$ is diverted directly into the inner tube via openings when it is fed in. Due to this flow of coolant, the inner tube acts like an ejector. Ejectors are jet pumps that suck in and transport a suction medium based on the pressure difference using the Venturi principle with the aid of an accelerated fluid jet [5]. The resulting lower pressure at the head of the tool in the inner tube causes the coolant-chip mixture to be sucked in. Suction of the coolant-chip mixture eliminates the need for a seal to the work-piece, making this deep hole drilling operation possible on conventional machining centers and eliminating the need for a special deep hole drilling machine with an oil feed apparatus and for a rear seal behind the workpiece. Moreover, with this configuration, the chips do not get in contact with the bore hole wall, thus improving the surface quality of the hole. The usual industrial diameter range for ejector deep hole drilling is between d = 18 mm and 65 mm [1].

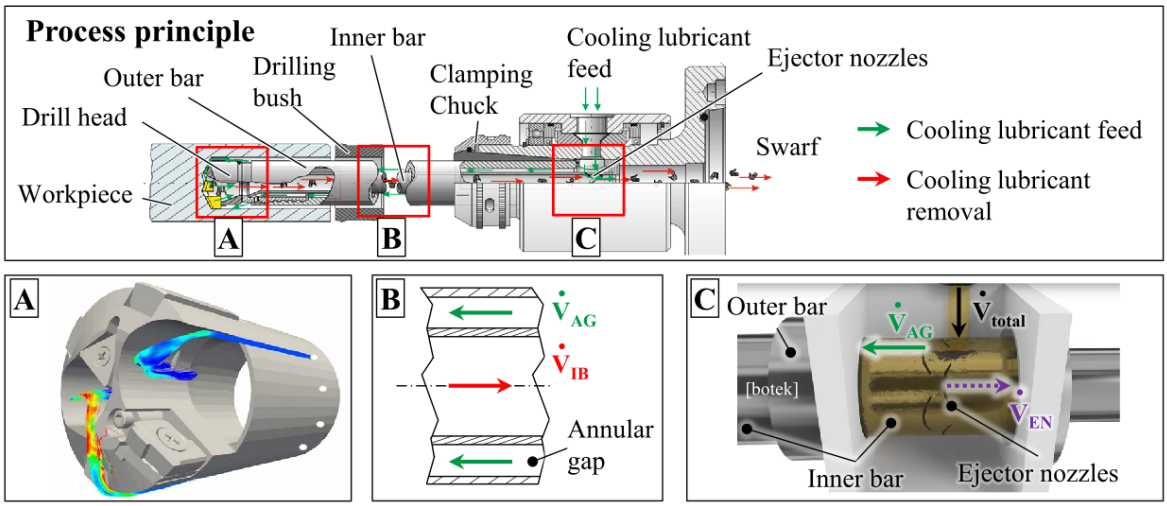

Figure 1: Schematic process principle ejector deep hole drilling; A) Drill head; B) Sectional view of the double tube system; C) Cooling lubricant feed system

Due to the special boundary conditions necessary for the existence of the ejector effect, the simulation of the flow combined with a production environment is essential to obtain the required knowledge. In this case, the simulation model is developed with the help of the mesh-free Smoothed Particle Hydrodynamics simulation method. There are three areas of major interest from the simulation point of view, both in term of physical results and of applicability of the SPH method: the feed area, shown in Fig. 1C, in which the lubricant is fed in the system and where the ejector effect takes place, the flow-exit area, in which the lubricant leaves the annular gap between inner and outer bar to reach the drill head, and the drill head area itself. In this paper the focus will be on the drill head area and on the flow-exit area.

3 SIMULATION ENVIRONMENT

The meaningful simulation of the events that occur in the process is fundamental to gain a deep understanding of all the characteristics and peculiarities of the system. The simulations in this work are developed applying the Lagrangian SPH method. This is a method for obtaining approximate numerical solutions of the partial differential equation, e.g., of fluid dynamics by replacing the fluid with a set of interpolation points, called particles, moving along with the fluid. One of the biggest advantages of this method is that it can handle flows with changing topology.

3.1 Applied SPH Formulation

In this work weakly compressible SPH is applied to solve the Navier-Stokes equations, that, in the Lagrangian form, are

$$\frac{\mathrm{d}\rho}{\mathrm{d}t} = -\rho\nabla\cdot\boldsymbol{v}, \tag{3}$$

$$\frac{\mathrm{d}\boldsymbol{v}}{\mathrm{d}t} = \frac{1}{\rho}\left(-\nabla p + \mu\nabla^2\boldsymbol{v} + \boldsymbol{f} + \nabla\boldsymbol{R}\right), \tag{4}$$

$$\frac{\mathrm{d}\boldsymbol{r}}{\mathrm{d}t} = \boldsymbol{v} \tag{5}$$

with ρ being the density, t the time, p the pressure, μ the dynamic viscosity, $\boldsymbol{r}$ the position, $\boldsymbol{v}$ the velocity, $\boldsymbol{f}$ the external forces, and $\boldsymbol{R}$ the Reynolds turbulent stresses.

Equation 3 implies that the fluid is not modelled as incompressible: a small fluctuation of the density is allowed. Applying an equation of state, a relation between density and pressure is built, and a quasi-compressible behavior is enforced by restoring a force which operates against the concentration of the fluid. In this work, the equation of state presented in [7] is applied

$$p = \frac{\rho_0 c_0^2}{\gamma}\left[\left(\frac{\rho}{\rho_0}\right)^{\gamma} - 1\right] + p_B \tag{6}$$

in which ρ_0 is the reference density, p_B the background pressure and the exponent γ is a scaling factor usually set to 7 for water. According to [6], in order to maintain stable and effective the computation, the reference velocity c_0 is set to be 10 time faster than the maximum expected velocity. The density fluctuations obtained with this constraint are limited to be less than 1%.

With the described formulation, the Navier-Stokes equations are transformed into a set of ordinary differential equations. The discretized approximation of the conservation of mass, Eq. 3, reads them

$$\frac{\mathrm{d}\rho_a}{\mathrm{d}t} = -\rho_a\sum_b \frac{m_b}{\rho_b}\boldsymbol{v}_{ab}\cdot\nabla_a W_{ab}, \tag{7}$$

where ρ_a and ρ_b are the densities of particles a and b, m_b is the mass of the particles, $\boldsymbol{v}_{ab} = \boldsymbol{v}_a - \boldsymbol{v}_b$ is the relative velocity and the term $\nabla_a W_{ab}$ is the gradient of the SPH kernel function, calculated with respect to the coordinates of particle a.

Although from the theoretical point of view all the particles of the fluid field interact with each other, from the approximative point of view only a certain number of particles has a relevant effect on the particle of reference. The interaction of particles is governed by a kernel function with compact support, also called smoothing function, that defines which particles are effectively interacting with the reference particles and also regulates the intensity of the interaction. For this work the Wendland kernel function [8] is chosen

$$W\left(\boldsymbol{r}_{ab}, h\right) = \alpha_D \left(1 - \frac{\mid \boldsymbol{r}_{ab} \mid}{2h}\right)^4 \left(2\frac{\mid \boldsymbol{r}_{ab} \mid}{h} + 1\right) \quad \text{for } 0 \leq \frac{\mid \boldsymbol{r}_{ab} \mid}{h} \leq 2 \tag{8}$$

with $\alpha_D = \frac{21}{16\pi h^3}$. The pressure term in Eq. 4 is approximated as

$$\nabla p_a = \rho_a \sum_b m_b \left(\frac{p_a}{\rho_a^2} + \frac{p_b}{\rho_b^2}\right) \nabla_a W_{ab} \tag{9}$$

with p_a and p_b being the pressure of particles a and b, while the viscous term, according to [9], is calculated as

$$\mu_a \nabla^2 \boldsymbol{v}_a = \rho_a \sum_b \frac{m_b \left(\mu_a + \mu_b\right) \boldsymbol{r}_{ab} \cdot \nabla_a W_{ab}}{\rho_a \rho_b \left(\parallel \boldsymbol{r}_{ab}^2 \parallel + 0.01h^2\right)} \boldsymbol{v}_{ab}, \tag{10}$$

where $\boldsymbol{v}_a$ is the velocity of particle a, h the SPH smoothing length, $\boldsymbol{r}_{ab}$ the distance between particle a and b, μ_a and μ_a are the dynamic viscosities of particles a and b. In order to stabilize the simulations, numerical parameters such as artificial viscosity and artificial pressure are adjusted according to the dynamic viscosity [10]. An artificial viscosity term is added [11]

$$\Pi_{ab} = \begin{cases} \dfrac{-\alpha \bar{c}_{ab} \mu_{ab} + \beta \mu_{ab}^2}{\bar{\rho}_{ab}} & \text{for } \boldsymbol{v}_{ab} \cdot \boldsymbol{r}_{ab} < 0, \\ 0 & \text{otherwise} \end{cases} \tag{11}$$

with the average density $\bar{\rho}_{ab} = \left(\bar{\rho}_a + \bar{\rho}_b\right)/2$, the average sound velocity $\bar{c}_{ab} = \left(\bar{c}_a + \bar{c}_b\right)/2$, and the artificial viscosity

$$\mu_{ab} = \frac{h \boldsymbol{v}_{ab} \cdot \boldsymbol{r}_{ab}}{\parallel \boldsymbol{r}_{ab}^2 \parallel + 0.01h^2}. \tag{12}$$

The parameters α and β are usually chosen to be close to $\alpha = 1$ and $\beta = 2$.

For the integration, an explicit second order predictor-corrector leapfrog integrator [12] is applied. The time step size Δt is controlled by the Courant-Friedrichs-Lewy conditions

$$\Delta t \leqslant \Delta t_{CFL} = \alpha \frac{h}{c_s}. \tag{13}$$

3.1.1 Boundary Treatment

Due to its mesh-free character, the SPH method can easily be coupled with other particle methods, such as the discrete element method. The algorithmic similarity of the methods allows an extremely efficient implementation of the SPH-DEM coupling without co-simulation and the associated problems, such as different integrators and step widths [13, 14]. With the help of this coupling, it is also possible to include very complex geometries with meshes consisting of triangles in the simulation without time-consuming mesh generation processes. In order to model the contact between fluid and boundary geometry, the possible contact pairings must be determined. The triangular meshes can then be coupled with SPH particles by a penalty approach, similar to the Lennard-Jones approach, as proposed in [15]. For the algorithm applied in this work, the penalty formulation implemented does not strive to infinity for vanishing distances between particles and triangles [16]. Being d the distance between the interacting particle and the triangle and R the maximum distance for which contact occurs, the resulting force F acting on the triangle's normal direction is

$$F(d) = \begin{cases} \psi \dfrac{(R-d)^4 - (R-s)^2(R-d)^2}{R^2 s(2R-s)} & \text{if } d \leq R, \\ 0 & \text{otherwise.} \end{cases} \tag{14}$$

The parameter s denotes the distance for which the force $F(d)$ switches from repulsive to attractive behavior, while the scalar ψ indicates the maximum absolute value at zero distance, i.e., $F(0) = \psi$.

3.1.2 Pasimodo

The simulations are performed with the software Pasimodo [17]. This software platform, developed since more than a decade at the Institute of Engineering and Computational Mechanics is used for many different applications [18, 19]. Its basic idea is to offer a general purpose highly modular framework for particle methods, written with the programming language C++, and structured in a highly object oriented environment. Pasimodo consists of a core and multiple plugins. The core, independent from the specific particle method applied, controls the basic steps necessary for every method. In the first step, the neighbour search, potential contact pairs are identified. In the second step, the forces to be exchanged between particles in a contact pair are evaluated. Lastly, during the integration step, particles are moved and their state variables are updated in accordance to the interaction evaluated in the previous steps. The plugins, compiled as shared libraries, can be programmed or modified without full knowledge of the core, and can be used to implement and combine almost arbitrarily different specific algorithms.

3.2 Modelling and simulation of the drilling system

Due to the complicated geometry and to the extremely small volumes in which the flow develops, it was necessary to adopt a very fine discretization of the fluid, leading to

extremely long computational times. For this reason, the flow-exit area and the drill head area are studied separately, considering the transient phase for the flow-exit area, when the fluid first approaches it, and the transient phase for the drill head area. Especially for the flow-exit area, not only the transient phase is important, since the steady state condition, after the whole available volume has been filled by lubricant, is crucial for the correct execution of the process. As mentioned before, no sealings are applied to the back of the drill system, thus just very small leakages are admissible, while still ensuring to provide the cutting area with an adequate lubricant flow.

First, the transient motion of the cooling lubricant at the flow-exit area is investigated. The drill considered has an external diameter $\phi_{ext} = 30$ mm, the inflow velocity is set to be $v_{in} = 60$ m/s, the particles are created in a Cartesian pattern with initial distance $x_{dist} = 3 \cdot 10^{-4}$ m and the smoothing length $h = 4.5 \cdot 10^{-4}$ m is used. This yields a total of about 75000 particles. The Courant-Friedrich-Lewy condition controls the time step size, which in average results to be $\Delta t = 1.403 \cdot 10^{-8}$ s for 0.001 s of the SPH simulation. The simulation considers, as a first approximation, a laminar flow approaching the area of interest, that is the area in which from the inner tube the lubricant flows to the external area of the drill head.

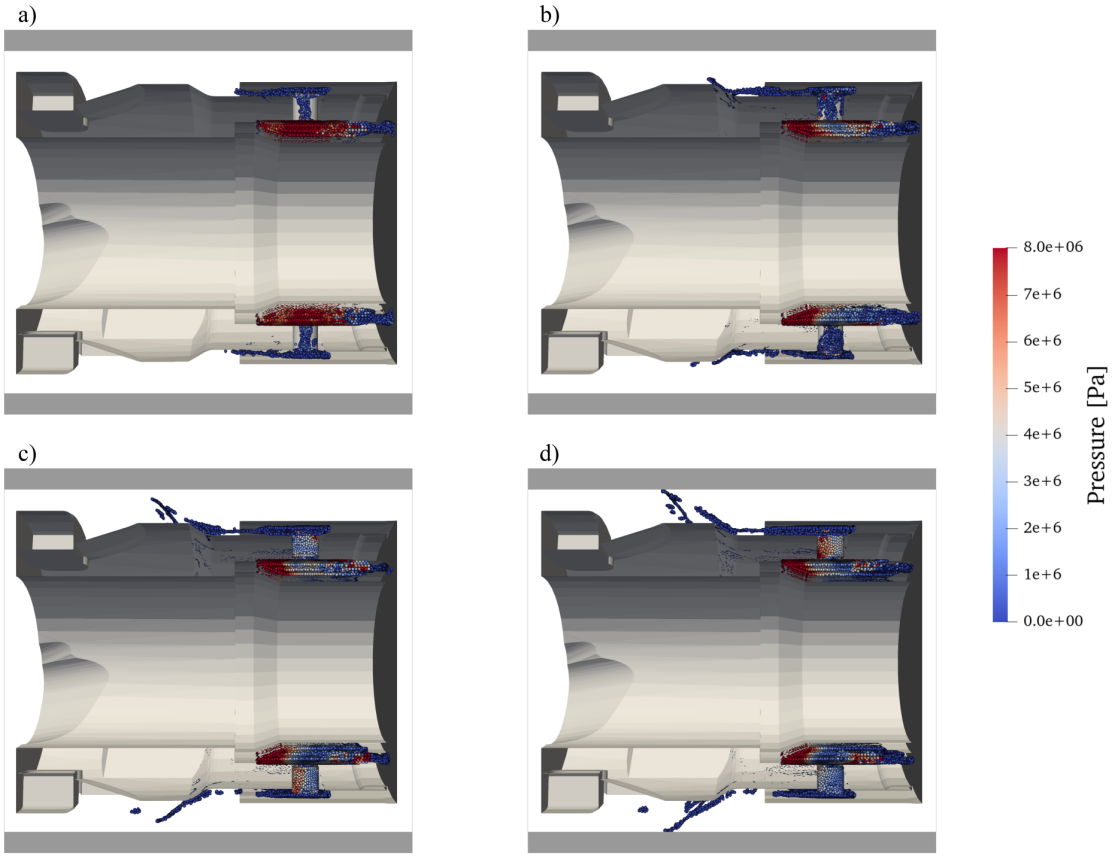

Figure 2: Transient evolution at the flow-exit area, sectional view. Evolution time: a) t=0.0005 s; b) t=0.0009 s; c) t=0.0011 s; d) t=0.0012 s.

Figure 2 shows the evolution in time of the fluid behaviour at the influx area. The available volume in the annular gap is already filled with lubricant that then starts to flow through the adduction holes (Fig. 2a). After the small gap with the outer bar is also filled (Fig. 2b,c), the lubricant flows towards the drill head (Fig. 2b,c,d). As predictable, the fluid flow presents some areas with little to zero fluid velocity and maximum pressure. The pressure distribution also ensures the correct evacuation of the fluid through the small adduction holes towards the outside of the drill body. As expected, during the transient phase no leakages are present yet, but of course the complete filling of the gap will determine the leakage flow.

The transient behavior of the cooling lubricant around the cutting head area is also investigated. Again, as a first approximation, a laminar flow approaching the cutting head area is considered. The inflow velocity is set, considering the standard flow rate of application and the results from the previuos simulation, to be $v_{in} = 11.4$ mm/s, the particles are created in a Cartesian pattern with initial distance $x_{dist} = 4 \cdot 10^{-4}$ m and smoothing length $h = 6 \cdot 10^{-4}$ m for a total of about 600000 particles. The time step size results to be in average $\Delta t = 5.46 \cdot 10^{-8}$ s for 0.01 s of the SPH simulation. Figures 3 and 4 show the flow evolution in time, around the drill head seen from inside and outside.

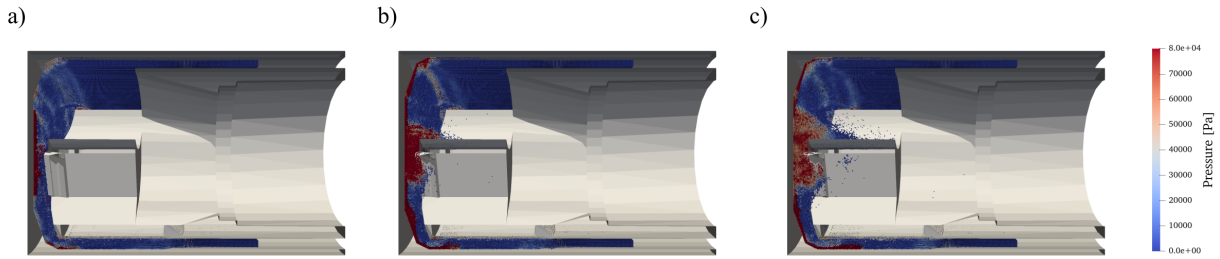

Figure 3: Transient evolution around the cutting edge, internal view at times: a) t=0.008 s; b) t=0.009 s; c) t=0.01 s.

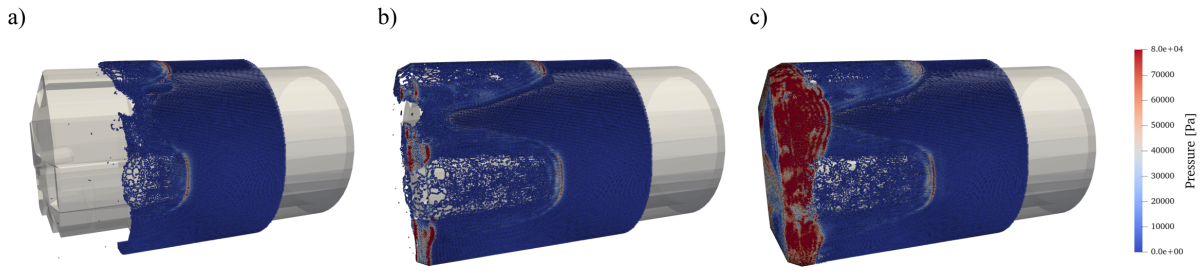

Figure 4: Transient evolution at the cutting edge, external view at times: a) t=0.004 s; b) t=0.006 s; c) t=0.008 s.

No problematic effects around the guide strips and the cutting edges are detectable. The flow is not excessively disturbed by the presence of this components and does not

present counterproductive tendencies to show extremely 'wild' motions. This behavior is crucial to ensure the stability of the flow in the whole system and the effectiveness of the ejector effect. The stability of the flow and of the ejector effect during the operation is fundamental for the adequate cooling of the drill and for the removal of the material while minimizing the quantity of fluid needed for the operation.

4 EXPERIMENTAL TEST STAND

The validation of the SPH simulations is performed with the help of experimental test series. For the test series, an ejector deep hole drilling system will be commissioned on an INDEX G250 five-axis machining center. For the analysis of the occurring physical effects in the running process, the system is extended with sensors. The machine and major components are sketched in Fig. 5. in the upper section. Due to the expected feed forces of approx. $F_f = 8 - 10$ kN, the ejector deep hole drilling system is mounted in the counter spindle of the machining center during drilling. The workpieces are clamped in the main spindle. The developed sensor setup allows in-process pressure and volume flow measurements during the deep hole drilling process with a rotating tool. Due to the high technical requirements, such as the fast rotation of the tool ($n \approx 950$ min^{-1}) and the resulting high acceleration forces (> 30g), the design of the double-tube system (difference in diameter of the annular gap between inner and outer bar $d_{Diff} = 1$mm), and the use in the fully flooded cooling lubricant area, the selection of suitable sensor technology in particular represents a major challenge. The positioning of the sensors is shown in the lower section of Fig. 5 in the sectional view of the CAD model.

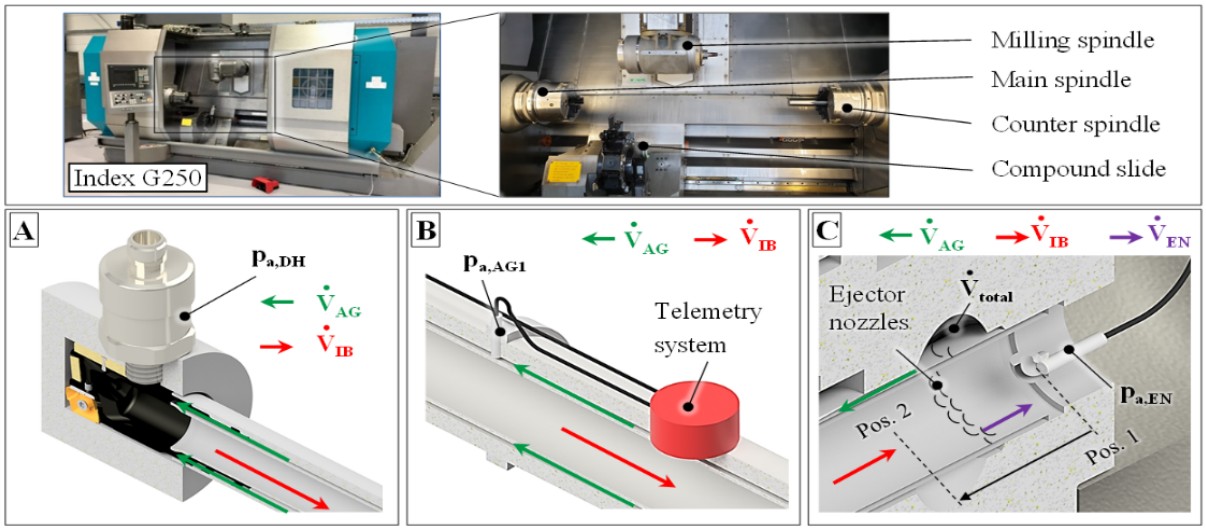

Figure 5: Adapted sensor system for static absolute pressure measurement on the ejector deep hole drilling system (drilling diameter d = 30 mm), A) pressure measurement in range of the drill head outlets B) pressure measurement in the annular gap C) Pressure measurement in front (pos. 1) and behind (pos. 2) the ejector nozzles in the inner bar

One of the objectives is to determine the volume flow distribution between the ejector

nozzles and the annular gap of the two bars, but due to the structure of the ejector system, flow sensors cannot be mounted at these positions. The volume flow rates to be investigated for the bore diameter $d = 30$mm are in the range of $\dot{V}_{feed} = 50 - 80$ l/min. As a substitute, the supplied volume flow $\dot{V}_{feed}$ into the system and the discharged total volume flows $\dot{V}_{IB}$ and $\dot{V}_{EN}$ are determined simultaneously. This not only shows the distribution of the volume flows and a potential leakage flow $\dot{V}_{loss}$, but also the point in time at which the ejector effect begins.

The pressure sensors are subject to the same conditions as the flow sensors. The resulting pressures in the system depend on the sensor position. Pressures in the range of $p = 10 - 20$ bar are expected in the overall system. To measure the pressure $p_{a,AG}$ in the annular gap between the inner and outer bar, the sensor must be radially fixed to the outer bar, (Fig. 5B). The challenge of radial mounting of the pressure sensors are the high acceleration forces and the data transmission of the rotating sensors. Miniature wired sensors by Kulite in combination with a Datatel telemetry system were selected. Due to the original field of application in turbomachinery, the manufacturer provides the measurement deviation as a function of acceleration forces, which allows measurement of the pressure under radial installation. The encapsulated design also allows the use of this sensor for pressure measurement in the flooded inner bar, (Fig. 5C). This requires the use of absolute pressure sensors, as no permanent contact with the ambient atmosphere can be guaranteed at this position [20]. With the help of an additively manufactured holder, the positioning of sensor $p_{a,EN}$ is variable. It can be positioned behind (position 1) and in front of (position 2) the ejector nozzles in the inner bar. Because of the non-rotating workpiece, standard pressure sensors can be used for the measurement in range of the drill head outlets (Fig. 5A). To make all measurements consistent, the absolute pressure of the fluid is also measured here. Due to the sensitivity of the telemetry system and the electronics, a protective device (telemetry chamber with cover and ring seal) against the cooling lubricant is required. The designed protection device is shown in Fig. 6. It allows the positioning of the required power supply (three 9V batteries) and telemetry transmitters on the clamping chuck of the ejector drill.

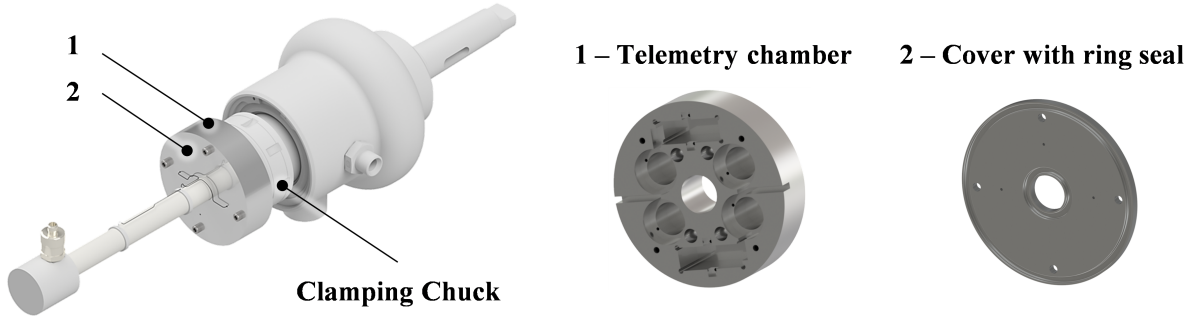

Figure 6: Telemetry chamber with cover and ring seal

5 CONCLUSIONS

In this paper, the joint simulation scheme and experimental test rig developed with the goal of obtaining a better understanding of the ejector deep hole drilling with a rotating tool are presented. The SPH method applied provides an effective tool for the simulation of the fluid flow in a complex geometry. The results presented confirm the reliability of the algorithm developed and the strength of the SPH method, when dealing with complex geometries and free surface flows with changing topologies, conditions particularly tough for standard finite element methods or finite difference methods. Moreover, a solid base for the study of the complete ejector drilling system was built: the physical parameters measured with the simulation provide a starting point for the comparison with the results obtained with the experimental rig, aiming to the development of a more accurate model for the drill and to an improvement of the simulation scheme.

ACKNOWLEDGEMENTS

Funded by the Deutsche Forschungsgemeinschaft DFG, (German Research Foundation) - Project number 439917965.

Tool data gently provided by botek Präzisionsbohrtechnik GmbH. The support is highly appreciated.

REFERENCES

[1] Biermann, D., Bleicher, F., Heisel, U., Klocke, F., Möhring, H.C. and Shih, A. Deep hole drilling. *CIRP Annals*. (2018) **67(2)**:673-694.

[2] Biermann, D., Kersting, M. and Kessler, N. Process adapted structure optimization of deep hole drilling tools. *CIRP Annals*. (2009) **58(1)**:89-92.

[3] Griffiths, B.J., Grieve and R.J. The role of the burnishing pads in the mechanics of the deep drilling process. *International Journal of Production Research*. (1985) **23(4)**:647-655.

[4] Deng, C.S., Huang, J.C. and Chin, J.H. Effects of support misalignments in deep-hole drill shafts on hole straightness. *International Journal of Machine Tools and Manufacture*. (2001) **41(8)**:1165-1188.

[5] Grazzini, G., Milazzo A. and Mazzelli, F. *Ejectors for efficient refrigeration*. Springer-Verlag, (2018).

[6] Monaghan, J.J. Smoothed Particle Hydrodynamics. *Reports on Progress in Physics*. (2005) **68(8)**:1703.

[7] Murnaghan, F.D. The compressibility of media under extreme pressures. *Proceedings of the National Academy of Sciences of the United States of America*. (1944) **30(9)**:244.

[8] Wendland, H. Piecewise polynomial, positive definite and compactly supported radial functions of minimal degree. *Advances in Computational Mathematics*. (1995) **4(1)**:389-396.

[9] Morris, J.P., Fox, P.J., and Zhu, Y. Modeling low Reynolds number incompressible flows using SPH. *Journal of Computational Physics*. (1997) **136(1)**:214-226.

[10] Schnabel, D., Özkaya, E., Biermann, D., Eberhard, P. Transient simulation of cooling lubricant flow for deep-hole drilling-processes. *Procedia CIRP*. (2018) **77**:78–81.

[11] Monaghan, J.J. Smoothed particle hydrodynamics. *Annual Review of Astronomy and Astrophysics*. (1992) **30(1)**:543-574.

[12] Monaghan, J.J., Kos, A. and Issa, N. Fluid motion generated by impact. *Journal of Waterway, Port, Coastal, and Ocean Engineering* (2003). **129(6)**:250-259.

[13] Gnanasambandham, C., Schönle, A., Eberhard, P. Investigating the dissipative effects of liquid-filled particle dampers using coupled DEM–SPH methods. *Computational Particle Mechanics*. (2019) **6(2)**:257-269

[14] Schnabel, D., Özkaya, E., Biermann, D., Eberhard, P. Modeling the motion of the cooling lubricant in drilling processes using the finite volume and the smoothed particle hydrodynamics methods. *Computer Methods in Applied Mechanics and Engineering*. (2018) **329**:369-395.

[15] Jones, J.E. On the determination of molecular fields. II. From the equation of state of a gas. *Proceedings of the Royal Society of London A: Mathematical, Physical and Engineering Sciences*. (1924) **106(738)**:463-477.

[16] Müller, M., Schirm, S., Teschner, M., Heidelberger, B. and Gross, M. Interaction of fluids with deformable solids. *Computer Animation and Virtual Worlds*. (2004) **15(3-4)**:159-171.

[17] Pasimodo, https://www.itm.uni-stuttgart.de/software/pasimodo/, last accessed June 7, 2021.

[18] Beck, F., Eberhard, P. Predicting abrasive wear with coupled Lagrangian methods. *Computational Particle Mechanics*. (2015) **2(1)**:51-62.

[19] Beck, F., Fleissner, F., Eberhard, P. Simulation of a pendulum with fluid interaction and experimental validation. *MARINE V: Proceedings of the V International Conference on Computational Methods in Marine Engineering*. (2013) CIMNE 479-490.

[20] Hesse, S., Schnell, G. *Sensoren für die Prozess- und Fabrikautomation*. Springer Vieweg, (2018).